# Facile Synthesis and Electrochemistry of Si-Sn-C Nanocomposites for High-Energy Li-Ion Batteries

Jing Xu,[a,=,c] Min Ling,[a,=] Lydia Terborg,[a] Hui Zhao,[a] Fen Qiu,[b] Jeffrey J. Urban,[b] Robert Kostecki,[a] Gao Liu,[a,*] and Wei Tong[a,*,z]

[a]*Energy Storage and Distributed Resources Division, Lawrence Berkeley National Laboratory, Berkeley, California 94720, USA*
[b]*The Molecular Foundry, Lawrence Berkeley National Laboratory, Berkeley, California 94720, USA*

Si-Sn-C nanocomposites were synthesized via a facile mechanical milling method. Phase composition and morphologies of the as-produced Si-Sn-C nanocomposites were characterized by X-ray diffraction (XRD), scanning electron microscopy (SEM), and Raman spectroscopy. Both XRD and Raman studies revealed the amorphization of Si after mechanical milling process, while Sn remained as the crystalline phase in both Si-Sn and Si-Sn-C nanocomposites. Meanwhile, the particle size was significantly reduced, but Si tended to agglomerate during the milling and it was alleviated through the addition of carbon. The galvanostatic charge/discharge measurements were carried out to evaluate the electrochemical performance. Compared to milled Si, Si-Sn nanocomposites, Si-Sn-C nanocomposites exhibited a higher initial capacity of ~1000 mAh/g, and its capacity was retained at ~80% after 50 cycles. The possible buffering effect of Sn and carbon at different operating potentials during the lithiation/delithiation process was discussed.

Li-ion battery technology has become one of the most promising energy storage solutions to power the plug-in hybrid-electric vehicles (PHEVs) and electric vehicles (EVs). Despite the current advances, the wide adoption of EVs is still being hindered by the battery performance and cost. Advances in both cathode and anode are needed in order to further enhance the energy density, extend the lifetime and reduce the cost.[1–3] Graphite anode used in the commercial Li-ion batteries has almost reached its theoretical capacity (372 mAh/g). Increasing the capacity of anode will essentially enable the use of less anode component, therefore, relieving the size and weight restrictions on batteries without impacting energy output, or vice versa.[4,5] For instance, doubling the energy density of anodes will increase the overall cell energy by about 20%.

Alternative metal-based anodes that are reactive with lithium to form alloys are well known for their high specific and volumetric capacity because of their ability to uptake more Li and better safety characteristics granted by the slightly higher operating potential vs. Li than graphite.[6,7] Of many metal candidates, Si holds the greatest promise because of its exceptionally high capacity, low cost, natural abundance, and environmental compatibility.[8–10] Upon reaction with lithium, Si material experiences an inhomogeneous and large volume change (>300%) in two-phase regions, causing cracking and/or pulverization of Si electrode, and loss of electrode integrity. As a result, Si electrode suffers from a large initial irreversible capacity and fast capacity decay over the extended cycles. Strategies to address these challenges mainly rely upon the development of nanostructured Si to accommodate mechanical strain and use of electrochemically active or inactive matrix to provide structural support.[11,12] Ideally, this component is electrochemically active and can act as a buffering and conductive matrix. Dahn's group performed extensive studies on various Si-based binary[13–15] and ternary[16–19] films using combinatorial sputtering method. They identified amorphous Si-Sn films with Sn content lower than 40 mol% as the ideal compositions in thin film batteries, for example, $Si_{0.66}Sn_{0.34}$ showed a large reversible capacity of ~1900 mAh/g and low irreversible capacity of ~100 mAh/g during the 1st cycle.[13] Ahn et al. later confirmed amorphous Si-Sn nanocomposite electrode films produced by magnetron co-sputtering method

demonstrated improved cycling performance compared to amorphous Si film at a similar thickness.[20] Sputtered films with phase separated amorphous Si embedded in the Sn matrix also delivered a reversible capacity of 1400 mAh/g with good cycling stability at Si/Sn ratio close to 1.[21] Attempt to prepare nanocomposites of Si/Sn-based nanoparticles enwrapped in porous carbon nanofibers was made by electro-spinning tetraethoxysilane/$SnCl_2$/polyacrylonitrile followed by heat-treatment. As-produced carbon and binder free Si/Sn@C electrode delivered an initial specific capacity of 1347 mAh/g and 1073 mAh/g was retained at the 50th cycle.[22] Kwon et al. reported a sophisticated synthesis of carbon-coated $Si_{70}Sn_{30}$ using butyl-capped analogues via firing at 900°C under vacuum. $Si_{70}Sn_{30}$ composite electrode exhibited a high reversible capacity of 2032 mAh/g and excellent capacity retention (97% after 60 cycles), which was attributed to the well-controlled particle size (<10 nm) and presence of carbon layer.[23] All the previous work showed the promising electrochemical performance within Si-Sn system, it would be interesting to apply a facile and scalable method to capitalize on the large theoretical capacity of Si, high electrical conductivity of Sn, as well as potential improvement in structural stability of the host electrode.[12]

In this work, we explored the synthesis of Si-Sn nanocomposites via mechanical milling method that is cost-effective, facile, and scalable. Typically, one can expect the following roles/functions out of ball milling process: (1) good/homogenous mixing; (2) particle size reduction; (3) mechanochemical reaction between precursors. The first two functions are generally applicable in most cases and the occurrence of mechanochemical reaction certainly varies with material chemistry. Using the base $Si_{0.66}Sn_{0.34}$ composition identified from the previous work,[13] we investigated the effect of milling energy and milling time on the particle size, morphology, and electrochemical properties. High energy milling method is effective in breaking down particle size when appropriate synthetic variables are used, for example, higher milling energy, longer milling duration, smaller balls etc. But the localized heat generated during milling process poses a challenge for the soft metals like Sn in either breaking down the particle size or reversely causing particle agglomeration. Therefore, we introduced the graphite during the synthesis and studied the electrochemistry of Si-Sn-C nanocomposites, to alleviate the agglomeration effect that is caused due to the low melting point (232°C) of Sn.[24,25] This paper presents the synthesis and electrochemistry of Si-Sn-C nanocomposites for the potential use as high-energy Li-ion anodes.

=These authors contributed equally to this work.
*Electrochemical Society Member.
cPresent address: Department of Materials Science and Engineering, Iowa State University, Ames, Iowa 50011, USA
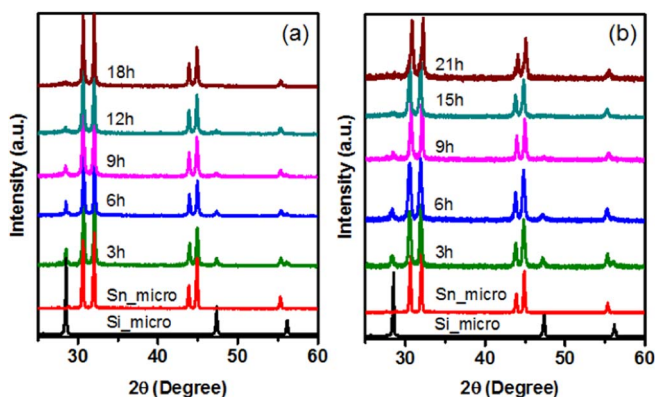zE-mail: weitong@lbl.gov

**Figure 1.** X-ray diffraction patterns of Si-Sn nanocomposites that were prepared by (a) planetary mill, (b) Spex mill for designated periods of time.

move the water solvent. Typical loadings of the active materials were around 0.5 mg/cm$^2$. 2325-type coin cells were assembled using Li metal as the counter electrode. 1.2 M LiPF$_6$ in ethylene carbonate: diethyl carbonate, 3:7 w/w containing 30 wt% fluoroethylene carbonate (FEC) (BASF) was used as the electrolyte. Galvanostatic discharge and charge at various current densities between 0.01 V and 1.00 V were performed on a Maccor 4200 battery cycler at 30°C. 1C was defined as 3000 mA/g in this work.

**Results and Discussion**

The synthesis of Si-Sn nanocomposites was performed on both Retsch planetary and Spex shaker mill. The Si and Sn precursors were milled for an extended period of time and the X-ray diffraction patterns were collected on a small amount of powder sample that was taken out of the milling vessel at a designated time. Several representative XRD patterns of Si-Sn nanocomposites are presented in Figure 1 along with those of micro-sized Si and Sn precursors as a reference. Overall, no mechanochemical reaction occurred between Si and Sn due to the immiscibility between Si and Sn. As can be seen in Figure 1, the intensity of the Si diffraction peaks started to decrease even after milling for 3 hours, suggesting Si phase tended to loose crystallinity during the high energy milling process. And Si ultimately became amorphous after milling for an extended period of time. It is worthwhile to point out that the precursors that were subjected to a planetary mill experienced a lower milling energy compared to those using a Spex mill because the frequency of impacts is much less in planetary mill despite its higher linear velocity of the balls. Therefore, a slight difference in Si crystallinity was observed in the final products when they were prepared by different mills even for the same period of time. On the contrary, we observed very little change in Sn, which remained as a high crystalline phase. This phenomenon appeared to be independent of milling energy and milling time. On the other hand, phase agglomeration was observed throughout the milling process and it became even more severe at a higher energy and longer milling time. Meanwhile, unlike the previous observation of Sn$_2$Fe phase resulting from the use of iron grinding media,[24,26] no Sn$_{1-x}$Fe$_x$ phase formation was noticeable throughout our experiments.

It is well known that the particle size is incredibly important and a particle size down to a few hundred nanometer is essential for metals to be used as Li-ion anodes.[11] We examined the microstructure of a few selected Si-Sn nanocomposite samples that were prepared by different energy/mill and period of time. They are denoted by the mill and milling time, for example, the sample Planetary_3 h suggested planetary milling for 3 hours. We started our synthesis with
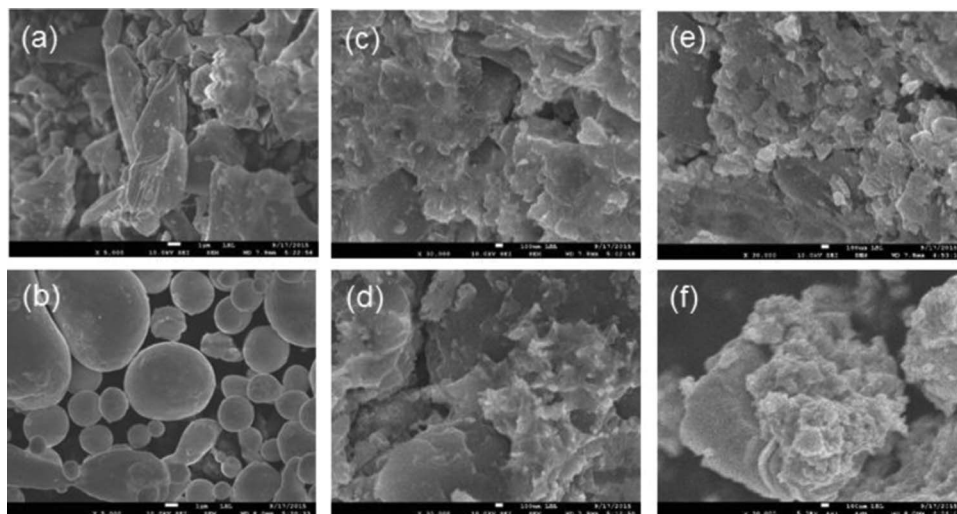
**Experimental**

Commercially available Si (325 mesh, Sigma Alrich) and Sn (10 μm, Sigma Aldrich) powder were used as precursors. The synthesis of Si-Sn and Si-Sn-C nanocomposites was performed on Retsch planetary mill (PM400, 400 rpm) and Spex shaker mill (Spex 8000M). Si and Sn precursors were loaded into the jar and sealed in an Ar-filled glove box and milling was performed with half an hour break for every 1.5 hours to minimize the accumulated heat during the milling process. X-ray diffraction (XRD) patterns were collected using a Bruker D2-Phaser with CuKα radiation (λ = 1.54178 Å). Scanning Electron Microscope (SEM) images were collected on a JEOL JSM-7000F and Zeiss Gemini Ultra-55 Analytical Field Emission SEM was used for imaging and elemental mapping. Raman spectroscopy was carried out using a "LabRAM" Raman microscope system (Horiba Jobin Yvon, USA) in a backscattering configuration coupled with an Ar-ion laser (Spectra Physics Inc., USA). The excitation wavelength was 488 nm. The Raman spectra were collected using an 80X microscope objective (Olympus America Inc., USA) with the laser power adjusted to ≤ 1 mW and a beam diameter at the sample of ca. 1 μm.

All the electrodes and coin cells were prepared and assembled in the Ar-filled glove box. Slurries containing 80 wt% of active material, 10 wt% of carboxymethyl cellulose binder, and 10 wt% Super C-65 (Timical) were prepared through a low energy ball milling process for 10 hours. The coated electrodes were placed in the glove box overnight and further dried under vacuum at 90°C for 12 hours to completely re-



**Figure 2.** SEM images of (a) Si precursor, (b) Sn precursor, (c) Planetary_3 h, (d) Planetary_12 h, (e) Spex_6 h, (f) Spex_15 h. Note the scale bar in (a, b) is 1 μm, and in (c, d, e, f) is 100 nm.
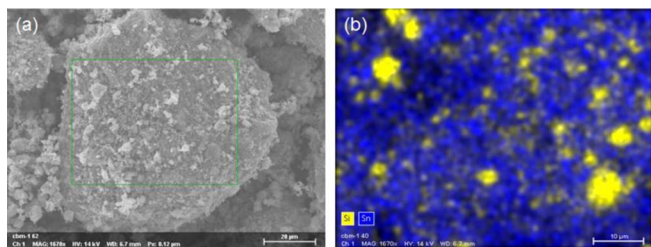
**Figure 3.** (a) SEM image, (b) Si, Sn EDS mapping of the selected area (outlined by green lines in (a)) in the as-prepared Si-Sn nanocomposites.



**Figure 4.** Raman spectra of (a) Si precursor, (b) Sn precursor, (c) Planetary_3 h, (d) Planetary_12 h, (e) Spex_6 h, and (f) Spex_15 h.

the commercially available Si and Sn precursors that have a relatively large particle size distribution between 1 and 10 μm (Figures 2a, 2b). As shown in Figures 2c, 2d, 2e, 2f, high energy milling process was very effective in breaking down the particle size. The spherical morphology of Si precursor disappeared; instead, all the selected Si-Sn nanocomposite samples have a much more reduced particle size compared to Si and Sn precursors. The primary particle size of Planetary_3 h sample (Figure 2c) is on the order of ∼500 nm, and increasing milling time (Figure 2d) and energy (Figures 2e, 2f) led to a further reduction to about 200 nm. However, inhomogeneous particle size distribution was evidenced by the presence of some large particles likely due to the particle agglomeration during the milling process (Figure 3a). Moreover, uneven elemental distribution of Si and Sn in the particle was observed (Figure 3b). We collected Energy dispersive X-ray spectroscopy (EDS) mapping on the representative particles. As shown in Figure 3b, some relatively large Si particles (yellow color) were clustered and embedded in the Sn matrix (blue color).

As revealed by XRD and SEM, the crystallinity and particle size of Si in the as-prepared Si-Sn nanocomposites were significantly reduced after high energy ball milling process. Raman spectroscopy is recognized as a suitable technique to analyze the vibrational properties of Si, in this context, it is used to study the effect of milling conditions on the crystallinity of Si (Figure 4). The optical vibrational modes of Si lattices are Raman active in the first order.[27] Highly crystalline Si has uniform bond angles and lengths, and the symmetrical Si-Si bonds result in strong Raman scattering. As shown in Figure 4, the Raman spectra of the Si precursor is featured by a sharp peak around 515 cm$^{-1}$, which is characteristic of homogeneous Si-Si bond vibration.[28,29] The sharp peak feature of Si was mostly retained in the as-prepared Si-Sn nanocomposite samples. A close examination of the Raman spectra revealed that the characteristic peak at 515 cm$^{-1}$ became broadened in the samples milled by planetary mill (Figures 4c, 4d) and a broad band centered around 480 cm$^{-1}$ that was associated with amorphous Si[28,29] was clearly distinguishable in the
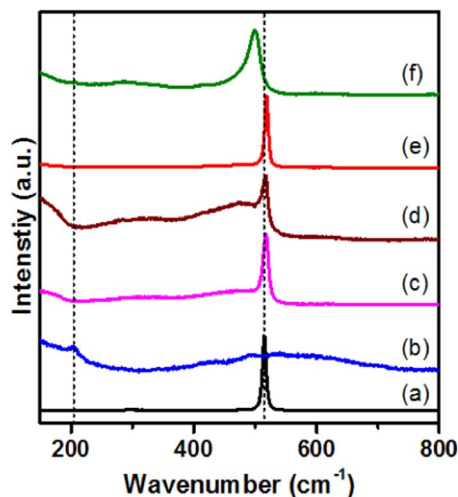
Planetary_12 h sample (Figure 4d). Meanwhile, a remarkable change in the Raman characteristic peak of Si appeared in Spex_15 h sample, which was evidenced by a significant shift to a lower wavenumber of about 500 cm$^{-1}$ along with a more pronounced degree of peak broadening (Figure 4f). Such strong downshift of Si-Si modes could be due to: (1) the deformation of the crystal lattice by the compressive stresses and the lattice defects that were generated by the high energy milling process,[30] (2) Si-Si vibration in proximity of Sn atoms,[31] (3) the presence of a large amount of amorphous Si due to the loss in the crystallinity of Si in Spex_15 h sample. Overall, the effect of milling conditions as revealed by Raman spectroscopy can be summarized as: Si tended to become amorphous at high milling energy and long milling time. This shows a good agreement with the XRD results. On the other hand, the collection of the Raman spectra of Sn was difficult due to the high absorption of light in the visible and near IR region in Sn.[32] From the Raman spectra of Sn precursor, we observe a very weak Raman peak around 200 cm$^{-1}$, which was assigned to be characteristic of Sn.[31,32] However, this feature was invisible in the as-milled nanocomposite samples. This invisible Raman feature of Sn was likely because it was hidden due to the presence of sharp Raman peak of Si in the spectra.

Guided by the structural and morphological characterization, the as-prepared Spex_15 h sample was selected for the electrochemical studies and the performance is presented in Figure 5. As shown in Figure 5a, it delivered an initial reversible capacity of about 650 mAh/g
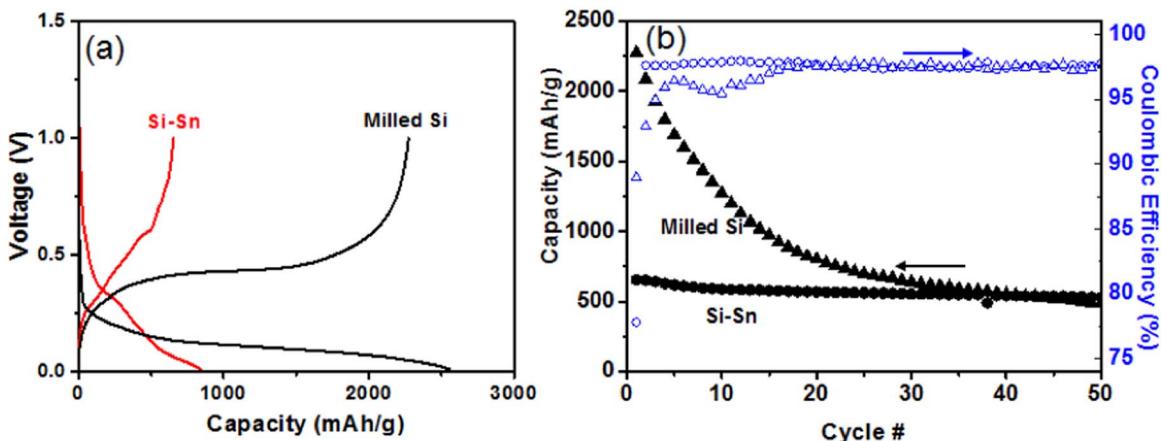


**Figure 5.** (a) The first cycle voltage profiles and (b) cycling performance of milled Si and Si-Sn nanocomposites.
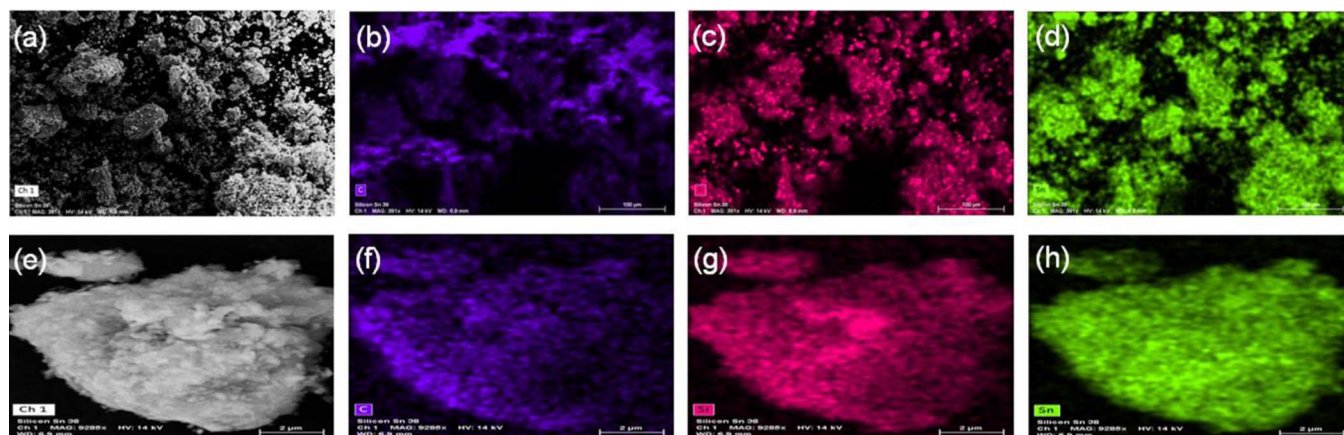
**Figure 6.** (a, e) SEM images, (b, f) EDS mapping of C, (c, g) EDS mapping of Si, (d, h) EDS mapping of Sn in Si-Sn-C nanocomposites. Note: (a - d) at lower magnification, (e - h) at higher magnification.

with the 1st cycle coulombic efficiency (CE) of 77.8%. The relatively low 1st cycle CE of Spex_15 h was likely resulted from the presence of crystalline Sn, which seemed to correlate with the inhomogeneity of the as-prepared sample as variation in electrode mass and capacity was observed. As a comparison, the electrochemical performance of Si, Sn precursors and milled Si were also tested. Both Si and Sn precursor exhibited poor electrochemical performance, e.g., low capacity (1500 mAh/g for Si, 300 mAh/g for Sn) and fast capacity decay, presumably due to the large particle size of these two precursors. For the sake of figure clarity, the electrochemical performance of these micro-sized precursors are not shown. On the other hand, Si precursor was milled under the same milling condition as Spex_15 h sample and used as a control sample. The reversible capacity of milled Si was increased to 2270 mAh/g (Figure 5a) as a result of significantly reduced particle size, but it showed a very fast capacity decay even in the early cycles (Figure 5b) due to the lack of buffering matrix (e.g., carbon) and possibly more side reactions with electrolyte. High energy milling process typically leads to smaller particle size and amorphous phase formation, however, when the particles are small enough, agglomeration between the small particles occurs.[33] Milled Si with much reduced particle size shortened the Li ion diffusion path and facilitate the alloying reaction between Li and Si, therefore, an increased capacity was observed. Meanwhile, the pulverization of the loosely agglomerated particles could occur after repeated volume change, even in the early cycles. On the contrary, it is interesting to observe that the Si-Sn nanocomposites demonstrated a better capacity retention, about 80% capacity was maintained after 50 cycles compared to milled Si.

To over counter the agglomeration problem, graphite was introduced during the high energy milling process because of its potential lubricating effect.[25] Use of electrochemically active and electronically conducting graphite that can be directly formulated into the electrode

eliminates an additional step to separate the final product and dispersing agent (e.g., organic liquid) that is typically introduced to alleviate the particle agglomeration during the milling process. More importantly, it removes a critical concern for the possible chemical reaction / modification on the surface of the electrode caused by the dispersing organic liquid. Meanwhile, milled Si was used as the precursor along with Sn and graphite in order to minimize the milling time for the preparation of Si-Sn-C nanocomposites. In this work, the Si-Sn-C nanocomposites containing 15 wt% graphite was prepared via a Spex mill. Overall, addition of carbon indeed alleviated the material agglomeration as no agglomeration was noticeable even after the precursors were milled for up to 12 hours. This was further confirmed by the EDS mapping for Si, Sn, and C as shown in Figure 6. As evidenced from EDS mapping, these three elements dispersed homogeneously and we did not observe obvious uneven elemental distribution, particularly for Si and Sn, at both large scale (Figures 6a–6d) and small scale (Figures 6e–6h). However, the addition of graphite did not bring an appreciable effect on reducing the crystallinity of Sn. On the other hand, the XRD patterns of as-prepared Si-Sn-C nanocomposites were very close, and increasing milling time did not result in any change in the Sn diffraction peaks that were still present as the main features (Figure 7a). The Si-Sn-C nanocomposites that was presented in Figures 7b, 7c were prepared by milling all precursors for 12 hours. In fact, we speculate that such a long milling time is not necessary to prepare homogeneously mixed nanocomposites. As shown in Figure 7b, addition of carbon improved the reversible capacity to about 1000 mAh/g and the 1st cycle coulombic efficiency of the as-prepared Si-Sn-C nanocomposites was increased to 80.2%. The capacity retention of Si-Sn-C nanocomposites was about 80% at Cycle 50, very close to that of Si-Sn nanocomposites. Such improvement could be ascribed to the following positive effects by adding carbon: (1) an increase
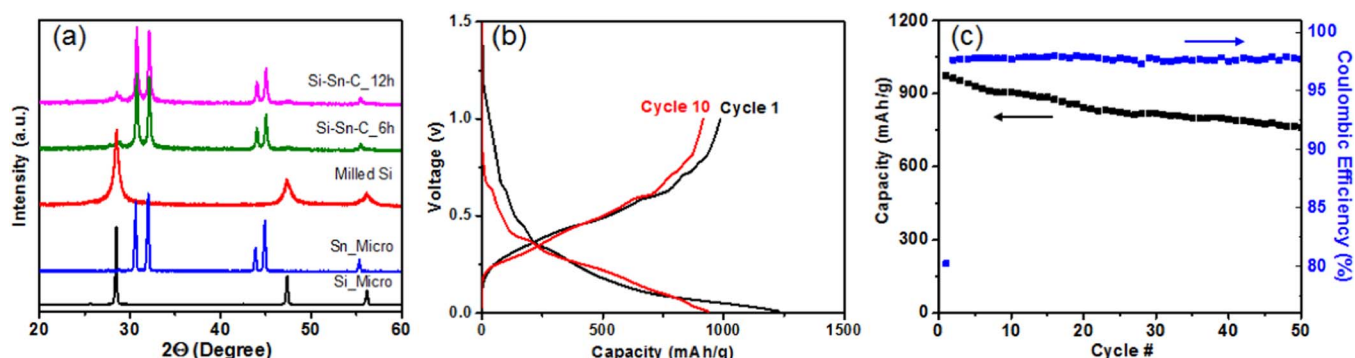


**Figure 7.** (a) XRD patterns, (b) voltage profiles, and (c) cycling performance of Si-Sn-C nanocomposites.
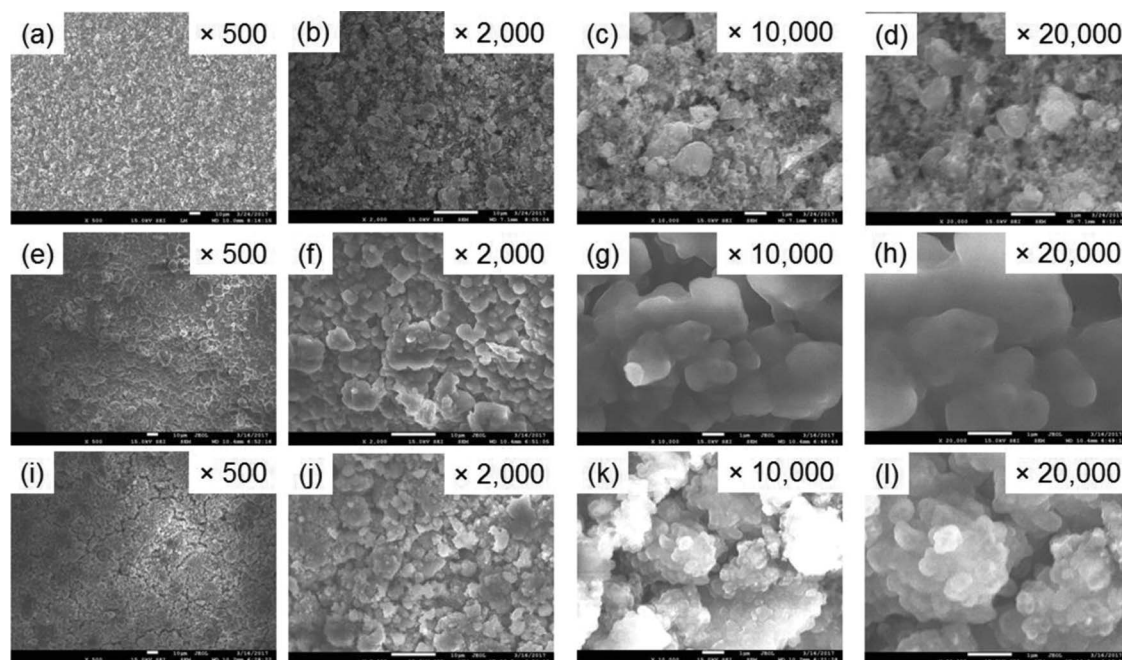
**Figure 8.** SEM images of Si-Sn-C electrodes at (a – d) pristine state, (e - h) the 50th lithiation, and (i - l) the 50th delithiation.

in electronic conductivity, (2) a minimal loss of electronic contact, and (3) its buffering effect. However, it was noticed that addition of carbon improved the reversible capacity, but the capacity retention of Si-Sn-C nanocomposite was similar to that of Si-Sn nanocomposites. This could be an indication of the mutual buffering effect between Si and Sn as their lithiation/delithiation occurs at slightly different potentials, because the buffering effect of carbon is expected to be less pronounced when more Li was involved in the lithiation/delithiation of Si-Sn-C nanocomposites due to the low carbon content in our Si-Sn-C nanocomposites sample.

To investigate the origin of the capacity loss, SEM images were collected on the Si-Sn-C electrodes at pristine state, the 50th lithiation, and the 50th delithiation (Figure 8). Comparing Figures 8a, 8e, 8i, we noticed the change in morphology on the electrode after 50 cycles, and some cracking occurred at the electrode level after the 50th delithiation. Electrode cracking was mainly due to the fact that both Si and Sn experiences volume changes during lithiation-delithiation process.[34–37] Such volume change was even more pronounced at higher magnifications. According to Figures 8d, 8h, 8l, the volumes of the particles significantly increased after lithiation, and the volumes cannot fully resumed back upon delithiation. Instead, the electrode became pulverized and led to additional side reactions between electrode and electrolyte, which largely accounted for the capacity loss over the extended cycles even at a lower electrode loading. This is believed to be a major contributing factor for capacity decay given the presence of a number of defects generated by high energy milling process.

Overall, in-depth studies on the physical and/or chemical properties of Si-Sn based electrodes that demonstrated a relatively good capacity retention compared to milled Si are under investigation to further isolate the role that each component plays during the electrochemistry. We speculate several possible factors could make contributions in kinetics and/or SEI formation, for example, amorphization of Si, particle size, and functionality of Sn etc. Synthesis of Si-Sn phases can be further explored for a proper control of the morphology, particle size and homogeneity, ideally, mixed Si and Sn at a small scale" via different synthetic techniques (e.g., melt spinning, chemical reduction method, etc.). In particular, chemical reduction method can enable the design of materials with controlled surface and bulk composition, i.e.,

core-shell structure, which will allow the in-depth understanding of the reaction mechanism of Si-Sn phases with lithium in the practical electrode..

## Conclusions

This work explored the synthesis of Si-Sn-C nanocomposites and its electrochemistry via a facile mechanical milling method. Both XRD and Raman spectroscopy showed the amorphization of Si, however, the challenge in synthesizing homogeneous Si-Sn nanocomposites via mechanical milling process was revealed presumably due to the low melting point of Sn. As a result, little change in Sn crystallinity was observed, which was independent of milling conditions. Electrochemical test of the as-prepared Si-Sn nanocomposites showed a reversible capacity of about 650 mAh/g and the capacity was retained at about 80% after 50 cycles. The relatively poor utilization of Si and Sn during the lithiation/delithiation process was attributed to the large agglomerated particles. To alleviate this problem, carbon was introduced to prepare Si-Sn-C nanocomposites. With the addition of carbon, no material agglomeration was observed and the as-prepared Si-Sn-C nanocomposites delivered an initial discharge capacity of about 1000 mAh/g and showed a similar capacity retention as Si-Sn nanocomposites. Despite numerous defects in the as-produced samples, the improved electrochemical performance of Si-Sn, and Si-Sn-C nanocomposites compared to milled Si suggests a potential avenue to search for high energy Li-ion anodes within ternary and quaternary Si-Sn based phases.

## References

1. V. Etacheri, R. Marom, R. Elazari, G. Salitra, and D. Aurbach, *Energ. Environ. Sci.*, **4**, 3243 (2011).
2. J. B. Goodenough and K. -S. Park, *J. Am. Chem. Soc.*, **135**, 1167 (2013).
3. J. B. Goodenough and Y. Kim, *Chem. Mater.*, **22**, 587 (2010).
4. S. Goriparti, E. Miele, F. De Angelis, E. Di Fabrizio, R. Proietti Zaccaria, and C. Capiglia, *J. Power Sources*, **257**, 421 (2014).
5. D. Andre, S. -J. Kim, P. Lamp, S. F. Lux, F. Maglia, O. Paschos, and B. Stiaszny, *J. Mater. Chem. A*, **3**, 6709 (2015).
6. C. -M. Park, J. -H. Kim, H. Kim, and H. -J. Sohn, *Chem. Soc. Rev.*, **39**, 3115 (2010).
7. N. Nitta and G. Yushin, *Part. Part. Syst. Char.*, **31**, 317 (2014).
8. H. Wu and Y. Cui, *Nano Today*, **7**, 414 (2012).
9. D. Larcher, S. Beattie, M. Morcrette, K. Edstrom, J. -C. Jumas, and J. -M. Tarascon, *J. Mater. Chem.*, **17**, 3759 (2007).
10. F. Luo, B. Liu, J. Zheng, G. Chu, K. Zhong, H. Li, X. Huang, and L. Chen, *J. Electrochem. Soc.*, **162**, A2509 (2015).
11. M. S. Whittingham, *Dalton Trans.*, 5424 (2008).
12. M. N. Obrovac and V. L. Chevrier, *Chem. Rev.*, **114**, 11444 (2014).
13. T. D. Hatchard and J. R. Dahn, *J. Electrochem. Soc.*, **151**, A1628 (2004).
14. M. D. Fleischauer, J. M. Topple, and J. R. Dahn, *Electrochem. Solid-State Lett.*, **8**, A137 (2005).
15. A. Timmons, A. D. W. Todd, S. D. Mead, G. H. Carey, R. J. Sanderson, R. E. Mar, and J. R. Dahn, *J. Electrochem. Soc.*, **154**, A865 (2007).
16. T. D. Hatchard, J. M. Topple, M. D. Fleischauer, and J. R. Dahn, *Electrochem. Solid-State Lett.*, **6**, A129 (2003).
17. M. D. Fleischauer and J. R. Dahn, *J. Electrochem. Soc.*, **151**, A1216 (2004).
18. M. A. Al-Maghrabi, J. S. Thorne, R. J. Sanderson, J. N. Byers, J. R. Dahn, and R. A. Dunlap, *J. Electrochem. Soc.*, **159**, A711 (2012).
19. M. A. Al-Maghrabi, V. L. Chevrier, J. R. Dahn, R. J. Sanderson, and R. A. Dunlap, *J. Electrochem. Soc.*, **164**, A498 (2017).
20. H. -J. Ahn, Y. -S. Kim, K. -W. Park, and T. -Y. Seong, *Chem. Commun.*, 43 (2005).
21. X. Xiao, J. S. Wang, P. Liu, A. K. Sachdev, M. W. Verbrugge, D. Haddad, and M. P. Balogh, *J. Power Sources*, **214**, 258 (2012).
22. H. Wang, H. Huang, L. Chen, C. Wang, B. Yan, Y. Yu, Y. Yang, and G. Yang, *ACS Sustain. Chem. Eng.*, **2**, 2310 (2014).
23. Y. Kwon and J. Cho, *Chem. Commun.*, 1109 (2008).
24. N. L. Rock and P. N. Kumta, *J. Power Sources*, **164**, 829 (2007).
25. N. Suresh Kumar Reddy and P. Venkateswara Rao, *Mater. Manuf. Processes*, **20**, 673 (2005).
26. R. Zhang, S. Upreti, and M. Stanley Whittingham, *J. Electrochem. Soc.*, **158**, A1498 (2011).
27. J. H. Parker, D. W. Feldman, and M. Ashkin, *Phys. Rev.*, **155**, 712 (1967).
28. A. T. Voutsas, M. K. Hatalis, J. Boyce, and A. Chiang, *J. Appl. Phys.*, **78**, 6999 (1995).
29. K. M. Ahn, S. M. Kang, and B. T. Ahn, *J. Electrochem. Soc.*, **158**, H374 (2011).
30. P. Unifantowicz, S. Vaucher, M. Lewandowska, and K. J. Kurzydłowski, *J. Phys.: Condens. Matter*, **20**, 025205 (2008).
31. J. -H. Fournier-Lupien, S. Mukherjee, S. Wirths, E. Pippel, N. Hayazawa, G. Mussler, J. M. Hartmann, P. Desjardins, D. Buca, and O. Moutanabbir, *Appl. Phys. Lett.*, **103**, 263103 (2013).
32. D. T. Wang, A. Göbel, J. Zegenhagen, and M. Cardona, *Phys. Rev. B*, **56**, 13167 (1997).
33. S. Fadda, A. Cincotti, A. Concas, M. Pisu, and G. Cao, *Powder Technol.*, **194**, 207 (2009).
34. Y. Xu, Y. Zhu, Y. Liu, and C. Wang, *Adv. Energy Mater.*, **3**, 128 (2013).
35. N. Li and C. R. Martin, *J. Electrochem. Soc.*, **148**, A164 (2001).
36. L. -F. Cui, R. Ruffo, C. K. Chan, H. Peng, and Y. Cui, *Nano Lett.*, **9**, 491 (2009).
37. U. Kasavajjula, C. Wang, and A. J. Appleby, *J. Power Sources*, **163**, 1003 (2007).